January 14, 2011

Wavelet Network for Semi-Active Control

Simon Laflamme, *Massachusetts Institute of Technology*
J.J.E. Slotine, *Massachusetts Institute of Technology*
J.J. Connor, *Massachusetts Institute of Technology*

Wavelet Network for Semi-Active Control

S. Laflamme, S.M. ASCE[1], J.J.E. Slotine[2], and J.J. Connor, F. ASCE[3]

Massachusetts Institute of Technology, Cambridge, MA 02139

laflamme@mit.edu, jjs@mit.edu, jjconnor@mit.edu

Abstract

This paper proposes a wavelet neurocontroller capable of self-adaptation and self-organization for uncertain systems controlled with semi-active devices, ideal candidates for control of large-scale civil structures. A condition on the sliding surface for cantilever-like structures is defined. The issue of applicability of the control solution to large-scale civil structures is made the central theme throughout the text, as this topic has not been extensively discussed in the literature. Stability and convergence of the proposed neurocontroller is assessed through various numerical simulations for harmonic, earthquake, and wind excitations. The simulations consist of semi-active dampers installed as a replacement to the current viscous damping system in an existing structure. The controller uses only localized measurements. Results show that the controller is stable for both active and semi-active control using limited measurements, and that it is capable of outperforming passive control strategies for earthquake and wind loads. In the case of wind load, the neurocontroller is found to also outperform an LQR controller designed using full knowledge of the states and system dynamics.

Subject Headings: wavelet, neural networks, structural control, adaptive systems, control systems, intelligent structures, large structures, vibration mitigation

1 Introduction

Integration of structural control in design can lead to significant savings by improving system responses to ensure occupant safety and structural integrity. For instance, the use of a tuned-mass damper (TMD) for the Citicorp Center in

[1]Ph.D. Candidate, Massachusetts Institute of Technology, Department of Civil and Environmental Engineering, 77 Massachusetts Avenue, Cambridge, MA, 02139, room #1-290 (corresponding author). E-mail: laflamme@mit.edu

[2]Professor of Mechanical Engineering and Information Sciences, Professor of Brain and Cognitive Sciences, Director of the Nonlinear Systems Laboratory, Massachusetts Avenue, Cambridge, MA, 02139, room #3-338.

[3]Professor of Civil and Environmental Engineering, Massachusetts Avenue, Cambridge, MA, 02139, room #1-253.

This is a manuscript of an article from ASCE, *Journal of Engineering Mechanics*, 137(7); 2011; 462-474. doi:10.1061/(ASCE)EM.1943-7889.0000248. Posted with permission.

New-York City saved 3.5 to 4 million dollars, which is the estimated cost of the additional quantity of steel that would have been required to satisfy the deflection criteria (Connor, 2003). Passive control techniques, such as TMD, base-isolation, hysteretic and viscous damping are now accepted by the industry and used in many buildings (Housner *et al.*, 1997; Spencer Jr and Nagarajaiah, 2003; Nitta *et al.*, 2006). Nevertheless, semi-active and active control schemes are not yet accepted nor widely implemented (Narasimhan and Nagarajaiah, 2005), despite significant research activity in the area. In recent work related to structural control, Ahlawat & Ramaswamy (Ahlawat and Ramaswamy, 2004) developed a fuzzy logic controller for active tuned-mass dampers, Wu *et al.* (Wu *et al.*, 2006) presented a controller designed for control of tall structures under wind excitations, Lin & Loh (Lin and Loh, 2008) studied semi-active control of base-isolation systems, Loh & Chang (Loh and Chang, 2008) studied centralized and decentralized control for civil structures. These active and semi-active systems are quite advantageous compared to passive strategies. They are effective for a wide range of excitations while some passive schemes, such as base-isolation, are only effective for limited bandwidth and do not perform well for near-field excitations (Yang and Agrawal, 2002).

Application of semi-active and active structural control strategies to civil structures is impeded by the following challenges: 1) high power requirement, and robustness in control in the case of a general power failure; 2) significant error on dynamic properties leading to inefficient controllers; and 3) limited state measurements (Yang *et al.*, 1995; Thai *et al.*, 1997; Wongprasert *et al.*, 2005). Considering the first problem, magnetorheological (MR) dampers are promising devices to achieve vibration mitigation as they only require a fraction of the power needed by active devices to achieve similar control performance (Spencer *et al.*, 1997; Jansen and Dyke, 2000). They can operate on batteries, which allows them to still function upon a general power failure, and are mechanically robust (Dominguez *et al.*, 2006). Despite their capabilities, MR devices and other semi-active devices face nontrivial problems: the challenge of developing robust algorithms to account for system uncertainties for full-scale implementation, plus the enhanced complexity of linking sensors to a large feedback system (Lynch *et al.*, 2008; Karamodin and Kazemi, 2010).

It is clear that these obstacles are obstructing the acceptability of semi-active devices. The applicability of semi-active control solutions has not been widely addressed by the research community (Ghaboussi and Joghataie, 1995; Xu, 2003; Soong and Cimellaro, 2009). Because the acceptability of this technology is inherently linked to its applicability, the development of an algorithm specialized for the civil engineering control problem is a fundamental step toward a broader implementation of semi-active systems.

The dynamic behavior of MR dampers has been successfully modeled using different approaches (Yang, 2001), but their complex dynamic behavior makes it difficult to map the required current or voltage for a desired force (Li and Chang, 2008). Even when such mapping is possible, knowledge of plant characteristics is required. However, dynamic characteristics of structures are inherently difficult to estimate accurately. Some controllers have been proposed to ac-

count for bounded uncertainties, such as sliding mode control (Yang *et al.*, 1995) and adapted LQR/H_2 control (Wang *et al.*, 2001), but the key issue is that a nominal estimation of the plant characteristics and a known bound on uncertainties are still required, and the controller performance depends on the level of these uncertainties. Neurocontrollers have been proposed to deal with uncertainties without prior knowledge of the plant. Sanner and Slotine (Sanner and Slotine, 1992) were the first to use Gaussian radial functions for active control of nonlinear systems. Cannon and Slotine (Cannon and Slotine, 1995) proposed to use adaptive wavelets for neurocontrol. For civil structures, neural nets have been used to map the entire plant/MR damper system (Fei and Xu, 2008; Shook *et al.*, 2009). However, classic neural networks must be trained a priori, which is difficult to achieve for large-scale structures.

Some effort has been made in the field of structural control to achieve adaptive control with semi-active devices. Hidaka *et al.* (Hidaka *et al.*, 1999) proposed an adaptive neural network controller for a three-story structure equipped with electrorheological dampers. The control strategy was composed of a predictive neural net and a controller neural net. The training scheme, however, necessitated the sets of input-output data from various types of excitation to apply batch training. Morishian *et al.* (Morishian *et al.*, 2003) proposed a neural network to control a three-story structure equipped with an MR damper. Similar to (Hidaka *et al.*, 1999), the strategy required batch training.

In work done for control using sequential learning, Zhou *et al.* (Zhou and Wang, 2003) used adaptive fuzzy control for a nonlinear base isolation system equipped with an MR damper. Their controller adapted sequentially. Lee *et al.* (Lee *et al.*, 2006) developed a semi active neurocontroller for base-isolation control with an MR damper, where the neural network was updated using a cost function and sensitivity evaluation. In their work, the cost function included the error on states, the control signal, and weighting matrices. Using weighting parameters, however, necessitates prior simulation or testing for their evaluation. Lee *et al.* (Jung *et al.*, 2007) achieved an adaptive modal neurocontroller for a structure equipped with an MR damper. This extension of (Lee *et al.*, 2006) used a Kalman filter to estimate modal states, and controlled the structure based on those states using the neurocontroller. Suresh *et al.* (Suresh *et al.*, 2008) proposed an adaptive mapping scheme that uses Gaussian radial functions to control base-isolation of nonlinear buildings equipped with an actuator. The proposed mapping has the advantage of a structure of self-learning during an event, while having the potential to use limited state measurements. A neurocontroller has been developed by the authors (Laflamme and Connor, 2009). The neural net is an inverse controller whose nodes sequentially adapt to achieve optimal control. The most significant contribution of the paper is the modification of the algorithm presented in Suresh *et al.* (Suresh *et al.*, 2008) to map the behavior of a civil structure equipped with semi-active devices, where adaptation is realized using a sliding controller and adaptive learning rates. A modified version of this controller (Laflamme *et al.*, 2009) includes an enhanced robustness in the adaptation laws and uses wavelets instead of Gaussian radial functions for a better functional localization.

Despite the fact that research geared towards adaptive control of MR damper seems to be limited in structural control, more has been done for car suspension mechanisms. Song *et al.* (Song *et al.*, 2005) proposed an adaptive controller for such mechanism. The controlled system was identified sequentially, and also included an adaptive controller in parallel. The research claimed to be the first to address the adaptive control of MR dampers with immeasurable nonstationary vibration sources, an applicability concern in the context of car suspension. System identification was achieved on a single degree-of-freedom system using a recursive least square (RLS) algorithm. However, the RLS algorithm tends to be less effective for systems with multiple degrees-of-freedom.

This paper proposes a wavelet neurocontroller capable of self-adaptation and self-organization. It is a controller designed for the class of dynamic systems characterized by large parametric uncertainties with an error bound that is unknown, or known to be very large. The intelligent controller is also adapted to systems controlled with semi-active devices characterized by having large sets of unreachable forces. Such devices are ideal candidates for structural control, as the large scale nature of the systems makes difficult the incorporation of active devices. The issue of applicability of the control solution to large-scale civil structures is made central throughout the text, as this topic has not been extensively discussed in the literature.

The paper is organized as follows: section 2 describes the neurocontroller. The general architecture of the controller is discussed, wavelet functions are introduced and used in the description of the self-organizing mapping as well as the self-adapting features. The section closes with discussions on inputs, time delay, measurement noise, and on the control objectives. Section 3 presents the MR damper theory, which is the semi-active device utilized in the simulations. Section 4 contains the numerical simulations to analyze the applicability, robustness and convergence of the controller. The simulations are conducted on an existing structure located in Boston, MA. They include active and semi-active mitigation of an harmonic excitation, and semi-active mitigation of earthquake and wind excitations. Section 5 concludes the paper.

2 Neurocontroller

The wavelet neurocontroller presented in this section is developed for control of dynamic systems with unknown dynamic parameters. Additionally, it is adapted for the case of control devices having uncertain force output. The force output error $\tilde{u}$ from those devices can be written:

$$\tilde{u} = u - u_{act} \tag{1}$$

where u is the required force output from the algorithm and u_{act} is the actual force output from the device. Example

of devices having such force uncertainties are low capacity actuators, semi-active systems, and some hybrid systems. The next subsections detail the proposed neurocontroller.

2.1 General Architecture

Neurocontrollers have the capability to control plants by mapping unknown nonlinear systems. As their name suggests, they are formed with neural networks, a mathematical representation based on the neurons consisting of a linear combination of different functions. Those functions are traditionally sigmoid and linear. Gaussian radial functions have been developed to replace traditional functions (Sanner and Slotine, 1992). Such neurocontrollers comprise several advantages compared to traditional neurocontrollers, among which are better approximation, convergence speed, optimality in solution and excellent localization (Suresh *et al.*, 2008). Those networks can also be trained more quickly than most other neural network techniques to model nonlinear systems by estimating in the function space (Sanner and Slotine, 1992; Kadirkamanathan and Niranjan, 1993; Howlett and Jain, 2001). Zhang *et al.* (Zhang *et al.*, 1992) introduced the concept of wavelet neural networks for system identification, and showed the wavelet capability to achieve universal approximation. Cannon & Slotine (Cannon and Slotine, 1995) proposed to use wavelet neural network for control. Hung *et al.* (Hung *et al.*, 2003) applied a wavelet neurocontroller for active control of a civil structure. Their neural net used batch training. In this paper, wavelet functions have been selected over Gaussian radial functions for their better space and frequency localization property. Unlike Gaussian functions, their locality in spatial frequency allows adaptive tuning of the functional approximation with respect to variations of the local spatial bandwidth of the controller (Cannon and Slotine, 1995). Thus, the training is quicker due to a more efficient representation.

The proposed neurocontroller is a direct inverse controller built to output forces based on state inputs, using a single hidden layer composed of radial wavelets. This hidden layer is capable of self-organization mapping, as well as self-adaptation. Self-organization mapping, developed by Kohonen (Kohonen, 1990), refers to the internal organization of nodes: nodes are added if the Euclidian distance of the input with respect to any existing node is larger than a certain threshold, and nodes can be pruned if judged unnecessary. Self-adaptation of nodes refers to the strategy of adapting nodal parameters.

The utilization of a self-adapting scheme arises from the choice of using sequential training rather than batch training, as batch training is difficult to achieve for large-scale systems because of the unavailability of input-output data sets. Sequential training consists of adapting the neurocontroller after each time step based on its performance. This is equivalent to changing the weight of the functions, along with the bandwidths and locations of wavelet functions. Among the adaptation algorithms for neural nets, such as back-propagation (BP), extended Kalman filtering, and re-

cursive least-square, the BP algorithms is superior in its computational simplicity (Behera *et al.*, 2006). Considering real-time control, the applicability of the neural controller requires computational simplicity and minimal data storage in order to avoid time delay. Noting that the BP scheme has slow convergence, time-varying learning rates are use to provide the neurocontroller with accelerated convergence for high magnitude dynamic responses. Training is slowed when the performance approaches a prescribed threshold, and stopped when the threshold is reached.

The neurocontroller maps the force output with respect to states. It results that the number of outputs corresponds to the number of actuators. The choice of state input is more involved. Prior knowledge of the system dynamics can improve the performance of the controller by specifying the types of inputs and the size of the lag space. This lag space has to be large enough to include the dynamics that properly describes the system, and to decide on an appropriate scaling of input which would improve the algorithm robustness and convergence speed (Nørgaard *et al.*, 2000). In the case of the proposed neurocontroller, the input vector consists of delayed measurements of localized dynamic states and force inputs. Its content for the simulations will be discussed in section 2.5.

As aforementioned, the main contribution of this paper is the design of an adaptive controller specialized for control devices with uncertain force output, such as semi-active devices. In their case, the force uncertainty arises from the incapacity to add energy to a system. The strategy is to let the neurocontroller adapt when it is in a desired control region C_d, a region where the uncertainty on the control device force output is minimum. This region is comprised within the general set C. When the system is outside C_d, the objective is to attempt bringing the system back in the desired region. This is achieved using a sliding controller. A third region, located at the boundary of C_d, is incorporated and acts as the transition region C_t to ensure a smooth transition between both control rules: $C \supset C_t \supset C_d$. This relationship is depicted in Fig. 1 for the case of an MR damper.

Fig. 2 shows a representation of the controller. The structure is excited by an external signal and the control device. Its dynamic states, as well as the damping forces, are fed in the adaptive neurocontroller. The neurocontroller outputs are fed in the sliding controller that adjusts the force based on the force reachability regions mentioned above. A voltage is then sent to the semi-active device based on the required force using a saturation rule, which will be defined later.

The next subsections describe the wavelet functions, followed by the self-organizing and the self-adaptive features, and a discussion on the choice of inputs, time delay, measurement errors, and the control strategies.

2.2 Wavelet Functions

The controller is a single layer neural net consisting of *mexican hat* wavelets ϕ of the form:

$$\phi(\boldsymbol{\nu}) = \left(1 - \frac{\|\boldsymbol{\nu} - \boldsymbol{\mu}\|^2}{\boldsymbol{\sigma}^2}\right) e^{-\frac{\|\boldsymbol{\nu}-\boldsymbol{\mu}\|^2}{\boldsymbol{\sigma}^2}} \tag{2}$$

where $\boldsymbol{\nu}$ is the input vector, $\boldsymbol{\mu}$ and $\boldsymbol{\sigma}$ are the center and bandwidth of the function respectively. The goal of the neurocontroller is to map the relationship between the control input and the output of the system. The output of the achieved representation from the neurocontroller, termed the desired force u_d, can be written:

$$u_{d,j}(\boldsymbol{\nu}) = \Sigma_{i=1}^{h} \alpha_{i,j} \phi_i(\boldsymbol{\nu}) = \boldsymbol{\alpha}_j^T \boldsymbol{\phi}(\boldsymbol{\nu}) \tag{3}$$

where $\alpha_{i,j}$ is the nodal weight i associated with the output j, h is the number of nodes in the hidden layer. Fig. 3(a) illustrates a *mexican hat* wavelet. Fig. 3(b) shows a single-layer feed-forward wavelet neural network.

For simplicity, the neurocontroller is specialized for a single device. The subscript j will be dropped. Note that this formulation holds for the case of decentralized controllers, which are used in the simulations.

2.3 Self-Organizing Mapping

The self-organizing feature of the neurocontroller consists of adding a node when the Euclidian distance of a new output to the closest node is farther than the threshold η. The network also has the capacity to prune nodes when their weights are found to be under a predefined ratio of the largest weight for several consecutive time steps. New nodes are added at the center of the new input, with the target weight α_i. Existing nodes are pruned if their weight fall below the threshold λ. The choice of α_i depends on λ. A function f can be mapped as a summation of wavelets by the frame operator F:

$$Ff = \langle f, \phi_i \rangle = \Sigma_{i=1}^{h} \phi_i f \tag{4}$$

where h represents the number of wavelet functions. Note that in the case of semi-active control, the function f is bounded, as civil structures equipped with such devices are inherently stable. The adjoint operator F^* is written:

$$\langle F^* \alpha, f \rangle = \langle \alpha, Ff \rangle = \Sigma_{i=1}^{h} \alpha_i \langle f, \phi_i \rangle \tag{5}$$

so that:

$$F^*Ff = \Sigma_{i=1}^{h} \langle f, \phi_i \rangle \phi_i \tag{6}$$

Therefore, a family of wavelets ϕ_i can be written in terms of a family of wavelets $\tilde{\phi}_i$ with zero mean:

$$\tilde{\phi}_i = (F^*F)^{-1}\phi_i \tag{7}$$

where the set $\tilde{\phi}_i$ is termed *dual frame*. Hence, the function f can be exactly reconstructed using coefficients:

$$\alpha_i = \langle f, \tilde{\phi}_i \rangle \tag{8}$$

Cannon and Slotine (Cannon and Slotine, 1995) show that, in order to prevent the addition of a node with an unrealistic weight that would result from a point sitting far from the existing function, the bound on α_i must be taken as:

$$|\alpha_i|_{max} = \alpha_0^{-d|\sigma|/2} |f|_{max} |\tilde{\phi}|_{max} \tag{9}$$

where α_0 is a scale parameter, d is the dimension of the separable wavelet families with scale α_0, f is the bound on the estimated functional and is equal to the bound on the control force u_b, and $|\tilde{\sigma}|_{max}$ is equal to the volume of the set C_t in the case of *mexican hat* wavelets. The scale parameter α_0 is taken from the dual frame family of radial wavelets that are written:

$$\tilde{\phi}_{i,(\sigma,\mu)} = \alpha_0^{-d|\sigma|/2} \tilde{\phi}_{i,(0,\mu)}(\alpha_0^{-d\sigma}\boldsymbol{\nu}) \tag{10}$$

where the subscript (σ, μ) denotes the scale σ of the dual set $\tilde{\phi}$ centered at μ, such that $\tilde{\phi}_{i,(0,\mu)}$ is a family of non-dilated wavelets centered at μ. Taking the minimum bound λ on the weights, it results that the bandwidth of the nodes from (9) is given by the expression:

$$\sigma_\lambda = \frac{2}{d \log a_0} \log\left(\frac{|u_b|C_t}{\alpha_i}\right) \leq \frac{2}{d \log a_0} \log\left(\frac{|u_b|C_t}{\lambda}\right) \tag{11}$$

From (11), it can be observed that reducing λ increases the approximation capability of the neural network.

The target nodal weight $\bar{\alpha}_i$ of a newly added node i is approximated using a weighted sum of the error. To enhance

stability, a smooth interpolation is incorporated when nodes are added:

$$\dot{\hat{\alpha}}_i = \begin{cases} \dot{\hat{\alpha}}_i & \text{if } |\alpha_i| \geq |\bar{\alpha}_i| \\ m_a(t)\alpha_i & \text{if } |\alpha_i| < |\bar{\alpha}_i| \end{cases} \tag{12}$$

where $\dot{\hat{\alpha}}$ is the parameter evolution according to the self adaptation rules described in the next subsection, and $m_a(t)$ is the smooth transition function infinitely differentiable and taken as the sigmoid function:

$$m_a(t) = \frac{1}{1 + e^{-at}} \tag{13}$$

with a being a positive constant.

2.4 Self-Adapting Feature

The adaptive rules of the neurocontroller are derived using Lyapunov stability to ensure robustness. Based on (3), the optimal mapping of control-input/state-output of the system equipped with a single MR damper can be expressed as:

$$u_d = \boldsymbol{\alpha}^T \boldsymbol{\phi} \tag{14}$$

where u_d is the desired (optimal) control force. The control law used herein is taken as:

$$\begin{aligned} u(t) &= (1 - m_c)\left(u_n - k \cdot \text{sat}\left(\frac{s}{\Phi}\right)\right) + m_c u_{sl} \\ &= (1 - m_c)\left(u_n - k \cdot \text{sat}\left(\frac{s}{\Phi}\right)\right) - m_c u_{max} \text{sat}\left(\frac{s}{\Phi}\right) \end{aligned} \tag{15}$$

where $u_n = \hat{\boldsymbol{\alpha}}^T \hat{\boldsymbol{\phi}}$ is the force output from the neurocontroller, the *hat* denotes estimated values, $u_{sl} = -u_{max}\text{sat}(s/\Phi)$ is the sliding component using the saturation function sat to bring the system back in subspace C_d, k is a constant, ϕ is a scaling parameter for the sliding surface, and m_c represents the control weight and is dependent on which subspace the system is located. Those terms will be mathematically defined later. The sliding surface s is taken as:

$$\begin{aligned} s &= \boldsymbol{P}\boldsymbol{e} = 0 \\ \dot{s} &= \boldsymbol{P}\dot{\boldsymbol{e}} = 0 \end{aligned} \tag{16}$$

where $\boldsymbol{e}$ is the error defined as the difference between the state $\boldsymbol{X}$ and the desired state $\boldsymbol{X}_d$, and $\boldsymbol{P}$ is a user-defined

vector. The selection of $\boldsymbol{P}$ will be discussed later.

Using (14), (15), the equation of motion of civil structure in the state-space representation:

$$\dot{\boldsymbol{X}} = \boldsymbol{A}\boldsymbol{X} + \boldsymbol{B}_u\boldsymbol{u} + \boldsymbol{B}_g a_g + \boldsymbol{B}_w\boldsymbol{w} \tag{17}$$

where $\boldsymbol{A}$ is the state-space matrix, $\boldsymbol{B}$ is the control force incidence vector with subscripts $\boldsymbol{u}$, $\boldsymbol{g}$, and $\boldsymbol{w}$ referring to actuation, ground excitation, and wind inputs respectively, a_g is the ground excitation input, and $\boldsymbol{w}$ is the wind excitation input, and substituting (1), the dynamics of the controlled state error can be written as:

$$\begin{aligned}
\dot{\boldsymbol{e}} &= \dot{\boldsymbol{X}} - \dot{\boldsymbol{X}}_{\boldsymbol{d}} \\
&= \boldsymbol{A}\boldsymbol{e} + \boldsymbol{B}(u_{act} - u_d + \epsilon) \\
&= \boldsymbol{A}\boldsymbol{e} + \boldsymbol{B}\left((1-m_c)\left(\hat{\boldsymbol{\alpha}}^T\hat{\boldsymbol{\phi}} - k\cdot\text{sat}\left(\frac{s}{\Phi}\right)\right) + m_c u_{sl} - \boldsymbol{\alpha}^T\boldsymbol{\phi} - \tilde{u} + \epsilon\right)
\end{aligned} \tag{18}$$

where the subscript d denotes the desired states, and ϵ is the estimation error. Note that the unknown external loadings a_g and $\boldsymbol{w}$ were in both right hand side terms of (18), thus canceled out.

To derive the adaptation rules, consider the following Lyapunov candidate using the sliding controller (Slotine and Coetsee, 1986):

$$V = \frac{1}{2}[s^2 + \tilde{\boldsymbol{\alpha}}^T\boldsymbol{\Gamma}_\alpha^{-1}\tilde{\boldsymbol{\alpha}} + \tilde{\boldsymbol{\phi}}^T\boldsymbol{\Gamma}_\phi^{-1}\tilde{\boldsymbol{\phi}}] \tag{19}$$

where Γ_α^{-1} and Γ_ϕ^{-1} are positive definite diagonal matrices representing learning parameters, and the tilde denotes the error between the estimated and real values ($\tilde{\boldsymbol{\alpha}} = \hat{\boldsymbol{\alpha}} - \boldsymbol{\alpha}; \tilde{\boldsymbol{\phi}} = \hat{\boldsymbol{\phi}} - \boldsymbol{\phi}$). It follows that (19) is positive definite and contains all time varying parameters. Neglecting the higher order term and specializing for the case where $s > \Phi$, the time derivative of V is:

$$\begin{aligned}
\dot{V} &= s\boldsymbol{P}\boldsymbol{A}\boldsymbol{e} + s\boldsymbol{P}\boldsymbol{B}(\hat{\boldsymbol{\alpha}}^T\tilde{\boldsymbol{\phi}} + \tilde{\boldsymbol{\alpha}}^T\hat{\boldsymbol{\phi}} - m_c\hat{\boldsymbol{\alpha}}^T\hat{\boldsymbol{\phi}}) + \tilde{\boldsymbol{\alpha}}^T\boldsymbol{\Gamma}_\alpha^{-1}\dot{\hat{\boldsymbol{\alpha}}} + \tilde{\boldsymbol{\phi}}^T\boldsymbol{\Gamma}_\phi^{-1}\dot{\hat{\boldsymbol{\phi}}} + \tilde{\boldsymbol{\alpha}}^T\boldsymbol{\Gamma}_\alpha^{-1}\tilde{\boldsymbol{\alpha}} \\
&+ \tilde{\boldsymbol{\phi}}^T\boldsymbol{\Gamma}_\phi^{-1}\tilde{\boldsymbol{\phi}} + s\boldsymbol{P}\boldsymbol{B}\epsilon - s\boldsymbol{P}\boldsymbol{B}\tilde{u} - (1-m_c)|s|\boldsymbol{P}\boldsymbol{B}k - s\boldsymbol{P}\boldsymbol{B}m_x u_{max}\text{sat}\left(\frac{s}{\Phi}\right) \\
&= \boldsymbol{e}^T\boldsymbol{P}^T\boldsymbol{P}\boldsymbol{A}\boldsymbol{e} + \tilde{\boldsymbol{\phi}}^T\left((1-m_c)\hat{\boldsymbol{\alpha}}^T\boldsymbol{B}^T\boldsymbol{P}^T s + \boldsymbol{\Gamma}_\phi^{-1}\dot{\hat{\boldsymbol{\phi}}}\right) + \tilde{\boldsymbol{\alpha}}^T\left((1-m_c)\hat{\boldsymbol{\phi}}^T\boldsymbol{B}^T\boldsymbol{P}^T s + \boldsymbol{\Gamma}_\alpha^{-1}\dot{\hat{\boldsymbol{\alpha}}}\right) \\
&- s\boldsymbol{P}\boldsymbol{B}(\tilde{u} - \epsilon) - (1-m_c)|s|\boldsymbol{P}\boldsymbol{B}k + \tilde{\boldsymbol{\xi}}^T\dot{\boldsymbol{\Gamma}}^{-1}\tilde{\boldsymbol{\xi}} - \tilde{\boldsymbol{\phi}}^T\boldsymbol{\Gamma}_\phi^{-1}\dot{\boldsymbol{\phi}} - s\boldsymbol{P}\boldsymbol{B}m_x u_{max}\text{sat}\left(\frac{s}{\Phi}\right)
\end{aligned} \tag{20}$$

with:

$$\tilde{\boldsymbol{\xi}} = \begin{bmatrix} \tilde{\boldsymbol{\alpha}} \\ \tilde{\boldsymbol{\phi}} \end{bmatrix}, \boldsymbol{\Gamma} = \begin{bmatrix} \boldsymbol{\Gamma}_\alpha & 0 \\ 0 & \boldsymbol{\Gamma}_\phi \end{bmatrix}$$

The *tilde* denotes the error between the optimal and current parameters, and $\boldsymbol{\xi}$ represents aggregation of parameters $\boldsymbol{\alpha}$ and $\boldsymbol{\phi}$. By choosing the following adaptation laws:

$$\begin{aligned} \dot{\hat{\boldsymbol{\alpha}}} &= -(1-m_c)(\boldsymbol{\Gamma}_\alpha \hat{\boldsymbol{\phi}})\boldsymbol{B}^T\boldsymbol{P}^T s \\ \dot{\hat{\boldsymbol{\phi}}} &= -(1-m_c)(\boldsymbol{\Gamma}_\phi \hat{\boldsymbol{\alpha}})\boldsymbol{B}^T\boldsymbol{P}^T s \\ \dot{\boldsymbol{\Gamma}}^{-1} &= -s^2\boldsymbol{I} \end{aligned} \tag{21}$$

where $\boldsymbol{I}$ is an identity matrix to populate $\dot{\boldsymbol{\Gamma}}^{-1}$, equation (20) becomes:

$$\dot{V} = \boldsymbol{e}^T\boldsymbol{P}^T\boldsymbol{P}\boldsymbol{A}\boldsymbol{e} - s\boldsymbol{P}\boldsymbol{B}(\tilde{u}-\epsilon) - (1-m_c)|s|\boldsymbol{P}\boldsymbol{B}k - \tilde{\boldsymbol{\xi}}^T(s^2\boldsymbol{I})\tilde{\boldsymbol{\xi}} - \tilde{\boldsymbol{\phi}}^T\boldsymbol{\Gamma}_\phi^{-1}\dot{\boldsymbol{\phi}} - s\boldsymbol{P}\boldsymbol{B}m_c u_{sl} \tag{22}$$

Choosing $k = u_b$, where u_b is a known bound (also positive) on $\tilde{u}$, (22) can be rewritten as:

$$\dot{V} = \boldsymbol{e}^T\boldsymbol{P}^T\boldsymbol{P}\boldsymbol{A}\boldsymbol{e} - s\boldsymbol{P}\boldsymbol{B}(\tilde{u}-\epsilon) - (1-m_c)|s|\boldsymbol{P}\boldsymbol{B}k - \tilde{\boldsymbol{\xi}}^T(s^2\boldsymbol{I})\tilde{\boldsymbol{\xi}} - \tilde{\boldsymbol{\phi}}^T\boldsymbol{\Gamma}_\phi^{-1}\dot{\boldsymbol{\phi}} - s\boldsymbol{P}\boldsymbol{B}m_c u_{max}\text{sat}\left(\frac{s}{\Phi}\right) \tag{23}$$

Defining mathematically the subspaces illustrated in Fig. 1:

$$\begin{aligned} C_d &= \{u_b \geq |\tilde{u}| \mid u_b, \tilde{u} \in \mathcal{R}\} \\ C_t &= \{u_b \geq \tau|\tilde{u}| \mid \tau \in [0,1], u_b, \tilde{u} \in \mathcal{R}\} \\ C &= \{\tilde{u} \mid \tilde{u} \in \mathcal{R}\} \end{aligned}$$

m_c is selected to make (23) as negative definite as possible:

$$\begin{aligned} m_c &= 0 && \text{if } \tilde{u} \in C_d \\ 0 < m_c &< 1 && \text{if } \tilde{u} \in C_t - C_d \\ m_c &= 1 && \text{if } \tilde{u} \in C - C_t \end{aligned} \tag{24}$$

Using (24), (23) can be rewritten:

$$\begin{aligned}\dot{V} &= \boldsymbol{e}^T\boldsymbol{P}^T\boldsymbol{P}\boldsymbol{A}\boldsymbol{e} - s\boldsymbol{P}\boldsymbol{B}(\tilde{u}-\epsilon) - |s|\boldsymbol{P}\boldsymbol{B}u_b - \tilde{\boldsymbol{\xi}}^T(s^2\boldsymbol{I})\tilde{\boldsymbol{\xi}} - \tilde{\boldsymbol{\phi}}^T\boldsymbol{\Gamma}_\phi^{-1}\dot{\boldsymbol{\phi}} \qquad \text{if } \tilde{u}\in C_d \\ \dot{V} &= \boldsymbol{e}^T\boldsymbol{P}^T\boldsymbol{P}\boldsymbol{A}\boldsymbol{e} - s\boldsymbol{P}\boldsymbol{B}(\tilde{u}-\epsilon) - |s|\boldsymbol{P}\boldsymbol{B}u_{max} - \tilde{\boldsymbol{\xi}}^T(s^2\boldsymbol{I})\tilde{\boldsymbol{\xi}} - \tilde{\boldsymbol{\phi}}^T\boldsymbol{\Gamma}_\phi^{-1}\dot{\boldsymbol{\phi}} \quad \text{if } \tilde{u}\in C-C_t\end{aligned} \tag{25}$$

The first term in (25) is negative semi-definite as the state-space matrix $\boldsymbol{A}$ is inherently stable for cantilever-like structures. Cantilever-like structures are here defined as series of mass systems joined by stiffness and damping systems, thus having stable eigenvalues. The third term is bigger than the second term for $\tilde{u}\in C_d$ and is as negative as possible for $\tilde{u}\in C-C_t$, and the fourth term is negative definite. The last term in (25) arises from the use of a sequential adaptive scheme, whereas the radial wavelet functions evolve with time. This term represents the trade-off in designing an adaptive neurocontroller for a system assumed to be fully uncertain. Using *Barbalat's lemma* and assuming that the first four terms are greater (in absolute value) than the last term, the error will converge to zero (Slotine *et al.*, 1991).

Noting that $\boldsymbol{P}^T\boldsymbol{P}$ is always semi-positive definite, the condition on the sliding surface coefficients $\boldsymbol{P}$ to ensure stability is that the dynamics of the sliding surface itself be stable. This is achieved for $\boldsymbol{P}$ being a Hurwitz polynomial, which is the condition on the sliding surface for cantilever-like structures. Thus, coefficients of $\boldsymbol{P}$ can conveniently be taken as all non-negative, with their values representing control weights analogous to the matrix $\boldsymbol{Q}$ in LQR control. Unavailable states can be represented by zero coefficients.

It can be noted that the switching law in (15), represented by the term k, can be used to control for system uncertainties. This is achieved by incorporating the error bound in k, thus augmenting the control weight of the error metric s, as shown in (Slotine *et al.*, 1991). However, selecting k requires the knowledge of the error bound. The largest uncertainty in (15) is the uncertainty of the error on the applied force u_b. This error can be quite large, and increasing its value too much would lead to a controller based almost exclusively on the sign of the sliding surface. Instead, a bound u_b is assumed, and adaptation on the network slowed or stopped when $|\tilde{u}| > u_b$. Note that this adaptation rate is directly related to the sliding controller as $k = u_b$. A sensitivity analysis of the controller with respect to u_b is included in the simulations.

The adaptation rules are in function of the matrix $\boldsymbol{B}$, assumed to be unknown. Since the magnitude of $\boldsymbol{B}$ can be easily evaluated and is of known sign, $\boldsymbol{B}^T\boldsymbol{P}^T$ can be incorporated in the learning rate. It follows that the adaptation rules (21) are a version of the BP algorithm as they are written in the form $\dot{\xi} = -\boldsymbol{\Gamma}_\xi\delta(\boldsymbol{\alpha}^T\boldsymbol{\phi})/\delta\xi\cdot s$. Therefore, without

loss of generality, the adaptation rules can be written in discrete form:

$$
\begin{aligned}
\hat{\alpha}_i(t+1) &= \hat{\alpha}_i(t) - \Delta(1-m_c)\Gamma_{\alpha_i}\hat{\phi}_i \text{sign}(\boldsymbol{B}^T\boldsymbol{P}^T)s \\
\hat{\mu}_{i,k}(t+1) &= \hat{\mu}_{i,k}(t) - \Delta(1-m_c)\Gamma_{\mu_{i,k}}\hat{\alpha}_i \left(\frac{1}{\sigma_i^4} e^{\frac{-\|\boldsymbol{\nu}-\mu_i\|^2}{\sigma_i^2}} \left(4\sigma_i^2(\nu_k-\mu_{i,k}) - 2\|\boldsymbol{\nu}-\mu_i\|^2(\nu_k-\mu_k)\right)\right) \\
&\qquad \cdot \text{sign}(\boldsymbol{B}^T\boldsymbol{P}^T)s \\
\hat{\sigma}_i(t+1) &= \hat{\sigma}_i(t) - \Delta(1-m_c)\Gamma_{\sigma_i}\hat{\alpha}_i \left(\frac{1}{\sigma_i^5} e^{\frac{-|\boldsymbol{\nu}-\mu_i\|^2}{\sigma_i^2}} (4\sigma_i^2\|\boldsymbol{\nu}-\mu_i\|^2 - 2\|\boldsymbol{\nu}-\mu_i\|^4)\right) \text{sign}(\boldsymbol{B}^T\boldsymbol{P}^T)s
\end{aligned}
\tag{26}
$$

where subscript k is the dimension of the neuron. Eq. (26) is the discrete adaptation law used for the simulations.

2.4.1 Adaptive Learning Parameters

Noting that $\boldsymbol{\Gamma}\boldsymbol{\Gamma}^{-1} = \boldsymbol{I}$, taking its time derivative results in:

$$
\dot{\boldsymbol{\Gamma}} = \boldsymbol{\Gamma}(s^2\boldsymbol{I})\boldsymbol{\Gamma} \tag{27}
$$

It is clear from (21) and (27) that the adaptive learning rate can be any increasing function, because $\dot{\boldsymbol{\Gamma}}^{-1}$ has to be semi negative definite. Using the sliding surface error in the function is intuitive, as a greater error indicates that the system is further from its optimality, therefore increasing the step taken in the descent direction. The need for rapidly increasing steps is only making engineering sense in the cases when quick learning is prescribed, such as for earthquake loads. In the case of wind load, those rates could be stationary. In order to prevent the learning rate from augmenting too quickly, and thus initiating system instability, (27) is modified by dividing by the 2-norm of the learning rate. Therefore, noting that in the following equation Γ_ξ is the ξ^{th}diagonal parameter of the matrix $\boldsymbol{\Gamma}$ and thus a scalar, the adaptation laws (21) for the ξ^{th}network parameter can be rewritten as:

$$
\begin{aligned}
\dot{\hat{\xi}} &= -\Gamma_\xi \left(\frac{\delta u}{\delta \xi}\right) \text{sign}(\boldsymbol{B}^T\boldsymbol{P}^T)s \\
\dot{\Gamma}_\xi &= s^2
\end{aligned}
\tag{28}
$$

2.5 Discussion on Inputs, Time Delay, and Measurement Errors

The sliding surface necessitates the knowledge of all displacements and velocities, as well as for some of the input vector in (2). To obtain those states, it is generally better to have an estimator. In practice, only accelerations are measured

because displacement and velocity measurements only provide relative quantities, are more expensive to measure than accelerations, and integration of acceleration can lead to significant errors (Jiménez-Fabián and Alvarez-Icaza, 2009). However, it can be shown that the phase space of a time series can be reconstructed using the delayed measurements of a single observation from the force inputs and the state outputs (Stark *et al.*, 2003; Kantz and Schreiber, 2004). Thus, a vector of acceleration measurements can contain the essential dynamics of a system, provided that it is properly constructed. Discussing techniques to construct such a vector is out of the scope of this manuscript. Instead, the idea is used to intuitively show that the acceleration inputs could be used as neural inputs as they give enough information on the current state of the controlled system, provided that the input vector is adequately constructed, or that it is large enough to enclose all of the essential dynamics. In other words, the inputs for the i^{th}WNN controller will consist of local acceleration measurements $\ddot{x}_i$ and force inputs u_i, delayed in time by a constant τ, and embedded in a dimension d:

$$\boldsymbol{\nu} = [\ \ddot{x}_i(t) \quad \ddot{x}_i(t-\tau) \quad ... \quad \ddot{x}_i(t-(d-1)\tau) \quad u_i(t) \quad u_i(t-\tau) \quad ... \quad u_i(t-(d-1)\tau)\ ] \tag{29}$$

For the proposed controller, the input states are the delayed measurements of accelerations and previously applied forces. Each control device has a decentralized controller that relies on local measurements only. The sliding surface is constructed using local displacement and velocity measurements. Hence, the vector $\boldsymbol{P}$ will contain null entries where measurements are not available. In the simulations contained in the next section, it is assumed that the control device displacements and velocities are measurable, which are related to inter-story states.

Time delay can induce instability in a control system (Connor, 2003). Even though the neurocontroller simulation time step remains under the sampling rate, the interaction sensor-controller-device will most likely induce a delay. If the delay is known, it can be implicitly fed in the neurocontroller by changing the lag time of each input. It can be also assumed that the neurocontroller will learn that the system has a delay, thus adapt. Measurement errors are also present in most controlled systems. An analysis of the controller performance with respect to time delay and measurement errors is included in the simulation section.

2.6 Discussion on the Control Objectives

It is important to understand the control objectives for civil structures in order to select appropriate network parameters. There exist two main regulatory control objectives: acceleration mitigation, and displacement mitigation. Acceleration mitigation is a serviceability criterion and is mostly applicable to moderate-to-high wind excitations. The evolution of the neurocontroller for acceleration mitigation can be achieved at a slow rate, as structural integrity is not of concern.

This allows higher robustness for the algorithm. Adaptive learning rates are switched off for acceleration control.

Displacement mitigation is a concern during earthquake excitations, as structural integrity is at stake, and it is fundamental to minimize stresses and strains in structural members. The controller needs to optimally adjust rapidly. Impulse-like excitations quickly send the system in a new set of states away from the initial states. An aggressive learning strategy is recommended as a result of the neural network being in a control region whose control rule has yet to be constructed. To overcome the robustness issue arising from using high learning rates, the controller is built to *forget* parts of the of the control rule that have been rapidly constructed (Grossberg, 1988). The strategy is to identify nodes that have been created following an impulse loading. An impulse region is identified when the norm of the sliding surface error rate of change goes beyond a threshold. In the impulse excitation region, the target weight α_i is considerably increased based on the error norm, and incrementally forgotten in the following time steps. Adaptive learning rates are switched on for displacement control.

3 Magnetorheological Dampers

The application of MR dampers for control of civil structures has attracted some attention in the research community since the 1990's. Despite some performance issues resulting from degradation of material properties (Avraam, 2009), their low power requirement, along with their mechanical robustness and fail-safe property make them potential candidates for vibration mitigation of large-scale systems. MR dampers are capable of generating a reaction force of 200 kN in 60 milliseconds, with a 50 W power input (Yang *et al.*, 2002). This semi-active device is used along with the proposed neurocontroller for the simulation presented in the next section. The force-displacement and velocity-displacement plots of an hypothetical 1350 kN MR damper for a periodic excitation are represented in Fig. 4.

The mathematical complexity of MR dampers results in a complex mapping of the required voltage for a desired force (Li and Chang, 2008). Some non-mathematical models have been proposed, such as adaptive identification, to map the relationship between the necessary voltages for desired forces (Terasawa *et al.*, 2004). Nevertheless, a saturation-type control rule for the voltage selection, which consists of applying full current in the MR damper if the magnitude of the required force is higher than and of the same sign of the magnitude of the damper force, and applying zero current otherwise, has shown excellent performance and simplicity (Jansen and Dyke, 2000; Yoshida *et al.*, 2003). For the simulations, that saturation rule is used when the damper dynamics is in its hysteresis region. Outside that region, the voltage input is computed based on the assumption that MR damper dynamics can closely be defined by the Bingham model. The Bingham model consists of a Coulomb friction element in parallel with a viscous

element (Spencer *et al.*, 1997). The MR force output f_{MR} in this region is therefore assumed to be:

$$f_{MR} = f_c(v) \cdot \text{sign}(\dot{x}) + c_0\dot{x} \tag{30}$$

where f_c is the Coulomb friction force and depends on the voltage input v, $\dot{x}$ is the device velocity, and c_0 is the viscous damping coefficient. The voltage is computed using (30) assuming $\dot{x}$ is measurable, which is a mild assumption as the state coincides with local relative measurements.

4 Simulation

A 39-story office tower located in downtown Boston, Massachusetts, as described in (McNamara and Taylor, 2003), is loaded in the X-direction in order to assess the performance of the proposed WNN. The building was equipped in the 1990's with fluid dampers in order to mitigate excessive acceleration levels produced by the proximity of an existing 52-story tower. Dampers are installed every other story from the 5thfloor up to the 34thfloor. The viscous dampers in the X-direction have a capacity of 1350 kN (300 kips) with a damping coefficient of 52550 kN·s/m (300 kips·s/in) below the 26th floor, and a capacity of 900 kN (200 kips) with a damping coefficient of 35000 kN·s/m (200 kips·s/in) from the 26th floor and above. In the simulation, viscous dampers have been replaced by MR dampers of similar capacities installed at the same locations. The equation of motion of the system can be written in the form of (17) where:

$$\boldsymbol{A} = \begin{bmatrix} \boldsymbol{O} & \boldsymbol{I} \\ -\boldsymbol{M}^{-1}\boldsymbol{K} & -\boldsymbol{M}^{-1}\boldsymbol{C} \end{bmatrix} \quad \boldsymbol{X} = \begin{bmatrix} \boldsymbol{x} \\ \dot{\boldsymbol{x}} \end{bmatrix}$$

$$\boldsymbol{B}_u = \begin{bmatrix} \boldsymbol{O} \\ -\boldsymbol{M}^{-1}\boldsymbol{F} \end{bmatrix} \quad \boldsymbol{B}_g = \begin{bmatrix} \boldsymbol{O} \\ -\boldsymbol{E} \end{bmatrix} \quad \boldsymbol{B}_w = \begin{bmatrix} \boldsymbol{O} \\ -\boldsymbol{M}^{-1}\boldsymbol{E} \end{bmatrix}$$

where $\boldsymbol{M} \in \mathcal{R}^{n\times n}, \boldsymbol{C} \in \mathcal{R}^{n\times n}$, and $\boldsymbol{K} \in \mathcal{R}^{n\times n}$ are the mass, damping, and stiffness matrices respectively, $\boldsymbol{I} \in \mathcal{R}^{n\times n}$ is the identity matrix, $\boldsymbol{F} \in \mathcal{R}^{n\times a}$ is the damper location matrix, $E \in \mathcal{R}^{n\times 1}$ is a vector of ones, n is the number of states, a is the number of actuators, and $\mathbf{0}$ are compatible zero matrices such that $\boldsymbol{A} \in \mathcal{R}^{2n\times 2n}$, $\boldsymbol{B}_u \in \mathcal{R}^{2n\times a}$, $\boldsymbol{B}_g, \boldsymbol{B}_w \in \mathcal{R}^{n\times 1}$, $\boldsymbol{X} \in \mathcal{R}^{2n\times 1}$, $u \in \mathcal{R}^{a\times 1}$, $a_g \in \mathcal{R}^{1\times 1}$, and $w \in \mathcal{R}^{n\times 1}$.

Three simulations are conducted. The first one consists of an harmonic excitation to show convergence of the error. The second simulation subjects the structure to the ElCentro 1940 North-South component earthquake to verify the performance of the proposed WNN to excitations containing impulse loads. The third simulation looks at the performance of the controller for wind mitigation to compare with results from (McNamara and Taylor, 2003).

For all simulations, decentralized control is used for each semi-active device installed between the $(i+1)^{\text{th}}$and the i^{th}floor. The assumed available measurements are inter-story displacements $x_{i+1} - x_i$, inter-story velocity $\dot{x}_{i+1} - \dot{x}_i$, acceleration $\ddot{x}_i$ and force input u_i. The sliding surface $\boldsymbol{P}$ is constructed accordingly. The force inputs for all simulations are scaled by a factor of 10^{-2} with respect to acceleration inputs.

4.1 Harmonic Load

A first set simulation is conducted using an harmonic excitation on the structure equipped with actuators in order to show the controller stability. The actuator is capable of outputting required forces within the range of the MR damper capacities, and saturates otherwise. Its dynamics is defined to be $\dot{u}_{act} = -(u_{act} - u_d)$. A similar dynamics is used for the voltage of the MR dampers. The harmonic excitation is a sinusoidal input at the fundamental frequency acting on every floor: $W(t) = 5 \sin 1.19t$. Results are compared with the structure equipped with MR dampers under the semi-active control. The controller non-adaptive parameters are kept constant for all simulations, except for the learning rates that have been multiplied by a factor of 10 for the semi-active case, due to the slower convergence caused by the sliding controller. The input vector has a time delay $\tau = 5$ and embedding dimension $d = 3$.

Fig. 5 shows the performance of the neurocontroller over 120 sec using the convergence of the error metric $\boldsymbol{Px}$. The transition zone slows the learning rates to 1% of their original values. The simulation results show that the WNN can stabilize a structure under an active control scheme, despite a slow convergence rate. The quick convergence of the semi-active controller is mainly a consequence of the excitation, where damping, thus higher voltage, favors mitigation. Fig. 6 shows the evolution of the control weights of the 15^{th}control device, for both the semi-active and active case. All weights converge. The semi-active control weights are mostly all positive, which results in an all-positive required control force. This is a consequence of the fact that the semi-active device cannot add energy to the structure, whereas an all-positive required force still stabilizes. The control weights of the active case have a symmetrical pattern.

A second analysis is conducted to verify the influence of time delay and measurement errors. Tables 1 and 2 show the maximum acceleration after $t = 120$ sec for the actuator and semi-active damper cases respectively. The results are in function of different control delay and measurement errors on both the acceleration and force outputs. The maximum acceleration has been taken as a performance indicator for convergence time, as all of the control cases converge. The delay consists of delaying the response of the control device, while the measurement errors consist of adding a noise. The noise has a Gaussian distribution.

Table 1 shows that the performance of the WNN improves slightly with control delay up to 400 ms, and then significantly deteriorates. The marginally enhanced convergence speed with delay can be a consequence of a better

input selection that results from a time delay, as the delay is equivalent to a time shift of the inputs. Table 2 also shows that the performance of the neurocontroller notably deteriorates with time delay, but no significant changes can be observed for small delays up to 400 ms. In both active and semi-active cases, the performance of the WNN does not seem to be sensitive to measurement error.

4.2 Earthquake Load

This section analyzes the performance of the controller under an earthquake-type excitation. The ElCentro 1940 North-South component earthquake (Chopra, 1995) is used due to its impulsive surges. The excitation has been scaled down to a maximum acceleration of 0.12 g. In this analysis, the performance of the controller is verified for inter-story displacement mitigation, and compared against other control strategies. Note that the existing viscous damping strategy was not designed for earthquake mitigation. The performance of the WNN is demonstrated under local state (LS) and full state (FS) measurements, and with the forgetting (F) and without the forgetting (NF) feature. A sensitivity analysis with respect to the error bound u_b is provided. The input vector is constructed with a time delay $\tau = 5$ and embedding dimension $d = 3$.

Table 3 shows the performance of the neurocontroller under various control strategies. Fig. 7 shows the maximum inter-story displacement profile from the 30thfloor to the roof. Floors 30-33 are representative of the lower floors. The viscous dampers case is the dampers currently installed in the tower. All non-adaptive parameters are kept constant throughout the simulation. The LS case uses local inter-story displacements and velocities at the damper locations, and the FS case assumes knowledge of all inter-story displacements and velocities. The performance of a LQR controller under full state and dynamics knowledge, as well as the FS cases, are indicated for benchmark purposes. The large discontinuity in inter-story displacements at the 36thfloor is caused by a drop in stiffness from the 35thfloor and above. The mass of the 39thfloor is 15% of the 38thfloor, which explains the small inter-story displacement of the 39thfloor.

Table 3 shows that the neurocontroller clearly outperforms all of the passive strategies for the optimal error bound $u_b = 675$ kN, with the performance of the WNN, LS, F case close to the LQR controller designed using full knowledge of the system dynamics. However, the controller is sensitive to u_b. While results tend to show that an optimal error bound exists, its high value signifies that an aggressive adaptation favors better mitigation. Such adaptation strategy for the WNN under chaotic and impulsive excitations is suited for semi-active control, because the control devices cannot destabilize the structure. Nevertheless, sequential and real-time adaptation under such excitation without knowledge of the controlled system is a challenging problem due to the very short training period and aggressive adaptation that may cause the network to step much beyond local minima during the gradient descent.

The WNN is not shown to perform better under full state measurement. This could be explained by the maximum

inter-story displacement being located at the 37thfloor, unreachable by the dampers. The use of the forgetting feature shows to give better mitigation performance.

Fig. 8 shows the evolution of network size for the 15thdamper, for $u_b = 675$ kN. Results show that using the forgetting feature results in networks that are significantly smaller. The network size between the LS case and the FS case, are similar with respect to the forgetting feature.

4.3 Wind Load

The last analysis has been conducted using a wind load such that the building responses under the uncontrolled case and the passive viscous cases compare with the one reported in (McNamara and Taylor, 2003). The selected input vector has a time delay $\tau = 10$ and embedding dimension $d = 3$. The performance from the current viscous damping strategy is used as a benchmark to evaluate the performance of the WNN.

The control objective is acceleration mitigation of the 37thfloor, which coincides with the largest acceleration among the occupied floors. Fig. 9 shows the maximum acceleration profile of the tower from the 30thfloor to the roof. Floors 30-33 are representative of the lower floors. Table 4 summarizes the maximum acceleration of the 37thfloor under various control strategies. Results show that the neurocontroller, both for LS and FS measurement strategies, outperforms all passive control strategies. The LS case performs better that the LQR controller designed using full knowledge, while the WNN FS case performs similar to the LQR controller. The excellent performance of the LS case with respect to the FS case may be a consequence of the damper placements. The FS case attempts to control for all degrees-of-freedom, but no control devices are located passed the 34thfloor. The floor above the 34thstory are not reachable in the control sense. The reader might appreciate that all semi-active control strategies significantly outperform the current viscous damping strategy using devices of similar capacities, which demonstrates the promise of semi-active control for civil structures.

5 Conclusion

A wavelet neurocontroller capable of self-adaptation and self-organization for uncertain or unknown systems controlled with semi-active devices has been presented. The neurocontroller has been simulated on an existing structure currently equipped with viscous dampers. In the simulations, the viscous damping strategy has been replaced by semi-active devices of similar capacities.

Simulations demonstrated promising performance for the neurocontroller using only local measurements. In the case of harmonic load, the WNN was capable of stabilizing the plant using active control, but high time delay resulted

in significantly slower convergence of the controller. The semi-active control case showed similar results. In both cases, measurement error did not significantly influence the performance of the system.

It was shown using the El Centro earthquake excitation that the controller was capable of a quick adaptation, and the inter-story displacement mitigation was better than the passive full voltage case, but worst than a LQR controller designed using full knowledge. The low performance relative to the LQR controller demonstrates that adaptive control of an uncertain system subjected to impulsive excitations without prior training is a challenging problem. The last simulation showed that the WNN is especially well suited for wind excitation. Acceleration reduction using the WNN was significantly better than any other control strategy. It was also demonstrated than semi-active control strategies gave better results than passive strategies.

References

Ahlawat, AS, and Ramaswamy, A. (2004). "Multiobjective optimal fuzzy logic controller driven active and hybrid control systems for seismically excited nonlinear buildings. ". *Journal of Engineering Mechanics*, **130**, 524–530.

Avraam, M. T. 2009. *MR-fluid brake design and its application to a portable muscular rehabilitation device*. Ph.D. thesis, Université Libre de Bruxelle, Bruxelle, Belgium.

Behera, L., Kumar, S., and Patnaik, A. (2006). "On adaptive learning rate that guarantees convergence in feedforward networks. ". *IEEE Transactions on Neural Networks*, **17**(5), 1116–1125.

Cannon, M., and Slotine, J.J.E. (1995). "Space-frequency localized basis function networks for nonlinear system estimation and control. ". *Neurocomputing*, **9**(3), 293–342.

Chopra, A.K. (1995). *Dynamics of structures*. Prentice Hall Englewood Cliffs, New Jersey.

Connor, J.J. (2003). *Introduction to structural motion control*. Prentice Hall New York.

Dominguez, A., Sedaghati, R., and Stiharu, I. (2006). "Semi-Active Vibration Control of Adaptive Structures Using Magnetorheological Dampers. ". *AIAA journal*, **44**(7), 1563–1571.

Fei, Y.Q.G.S.M., and Xu, Z.D. (2008). "Simulation Analysis on Intelligent Structures with Magnetorheological Dampers. ". *Journal of intelligent material systems and structures*, **19**(6), 1–12.

Ghaboussi, J., and Joghataie, A. (1995). "Active control of structures using neural networks. ". *Journal of Engineering Mechanics*, **121**(4), 555–567.

Grossberg, S. (1988). “Nonlinear neural networks: Principles, mechanisms, and architectures. ”. *Neural Networks*, **1**(1), 17–61.

Hidaka, S., Ahn, Y.K., and Morishita, S. (1999). “Adaptive vibration control by a variable-damping dynamic absorber using ER fluid. ”. *Journal of Vibration and Acoustics*, **121**, 373–378.

Housner, G.W., Bergman, LA, Caughey, TK, Chassiakos, AG, Claus, RO, Masri, SF, Skelton, RE, Soong, TT, Spencer, BF, and Yao, JTP. (1997). “Structural control: past, present, and future. ”. *Journal of Engineering Mechanics*, **123**(9), 897–971.

Howlett, R.J., and Jain, LC. (2001). *Radial basis function networks 1: recent developments in theory and applications*. Physica Verlag.

Hung, S.L., Huang, CS, Wen, CM, and Hsu, YC. (2003). “Nonparametric identification of a building structure from experimental data using wavelet neural network. ”. *Computer-Aided Civil and Infrastructure Engineering*, **18**(5), 356–368.

Jansen, L.M., and Dyke, S.J. (2000). “Semiactive control strategies for MR dampers: comparative study. ”. *Journal of Engineering Mechanics*, **126**(8), 795–803.

Jiménez-Fabián, R., and Alvarez-Icaza, L. (2009). “Simultaneous state estimation and parameter tuning in a shear building with a magneto-rheological damper. ”. *Structural Control and Health Monitoring*, **16**(4), 483–502.

Jung, H.J., Lee, H.J., Cho, S.W., and Lee, I.W. (2007). “An Experimental Study of Semiactive Modal Neuro-control Scheme Using MR Damper for Building Structure. ”. *Journal of intelligent material systems and structures*, **19**(9), 1005–1015.

Kadirkamanathan, V., and Niranjan, M. (1993). “A function estimation approach to sequential learning with neural networks. ”. *Neural Computation*, **5**(6), 954–975.

Kantz, H., and Schreiber, T. (2004). *Nonlinear time series analysis*. Cambridge Univ Press.

Karamodin, A., and Kazemi, H. (2010). “Semi-active control of structures using neuro-predictive algorithm for MR dampers. ”. *Structural Control and Health Monitoring*, **17**(3), 237–253.

Kohonen, T. (1990). “The self-organizing map. ”. *Proceedings of the IEEE*, **78**(9), 1464–1480.

Laflamme, S., and Connor, J.J. 2009. “Application of self-tuning Gaussian networks for control of civil structures equipped with magnetorheological dampers. ”. *Page 72880M of: Proceedings of SPIE*, vol. 7288.

Laflamme, S., Yu, T.-Y., and Connor, J.J. 2009. “Intelligent Controller for Smart Base Isolation of Masonry Structures. ”. *Pages 37–46 of: Proceedings of International Workshop on Smart Materials and Structures*.

Lee, H.J., Yang, G., Jung, H.J., Spencer, B.F., and Lee, I.W. (2006). “Semi-active neurocontrol of a base-isolated benchmark structure. ”. *Structural Control and Health Monitoring*, **13**(2-3), 682–692.

Li, H.N., and Chang, Z.G. (2008). “Semi-active control for eccentric structures with MR damper based on hybrid intelligent algorithm. ”. *The Structural Design of Tall and Special Buildings*, **17**(1), 167–180.

Lin, P.Y., and Loh, C.H. 2008. “Semi-active control of floor isolation system using MR-damper. ”. *Page 69320U of: Proceedings of SPIE*, vol. 6932.

Loh, C.H., and Chang, C.M. (2008). “Application of Centralized and Decentralized Control to Building Structure: Analytical Study. ”. *Journal of Engineering Mechanics*, **134**, 970–982.

Lynch, JP, Wang, Y., Swartz, RA, Lu, KC, and Loh, CH. (2008). “Implementation of a closed-loop structural control system using wireless sensor networks. ”. *Structural Control and Health Monitoring*, **15**(4), 518–539.

McNamara, R.J., and Taylor, D.P. (2003). “Fluid viscous dampers for high-rise buildings. ”. *The Structural Design of Tall and Special Buildings*, **12**(2), 145–154.

Morishian, S., Shiraishi, T., and Nakaya, N. 2003. “Adaptive Vibration Control of a Structure using MR Damper. ”. *Pages 761–766 of: Proceedings of the Third World Conference on Structural Control*.

Narasimhan, S., and Nagarajaiah, S. (2005). “A STFT semiactive controller for base isolated buildings with variable stiffness isolation systems. ”. *Engineering structures*, **27**(4), 514–523.

Nitta, Y., Nishitani, A., and Spencer Jr, B.F. (2006). “Semiactive control strategy for smart base isolation utilizing absolute acceleration information. ”. *Structural Control and Health Monitoring*, **13**(2-3), 649–659.

Nørgaard, M., Ravn, O., Poulsen, N.K., and Hansen, L.K. (2000). *Neural networks for modelling and control of dynamic systems: A practitioner’s handbook*. Springer Verlag.

Sanner, R.M., and Slotine, J.J.E. (1992). “Gaussian networks for direct adaptive control. ”. *IEEE Transactions on Neural Networks*, **3**(6), 837–863.

Shook, D.A., Roschke, P.N., Lin, P.Y., and Loh, C.H. (2009). “Semi-active control of a torsionally-responsive structure. ”. *Engineering Structures*, **31**(1), 57–68.

Slotine, J.J.E., and Coetsee, JA. (1986). “Adaptive sliding controller synthesis for non-linear systems. ”. *International Journal of Control*, **43**(6), 1631–1651.

Slotine, J.J.E., Li, W., *et al.* (1991). *Applied nonlinear control*. Prentice Hall Englewood Cliffs, NJ.

Song, X., Engineer, P., Ahmadian, M., Southward, S., Miller, L.R., *et al.* (2005). “An adaptive semiactive control algorithm for magnetorheological suspension systems. ”. *Journal of Vibration and Acoustics*, **127**, 493–502.

Soong, TT, and Cimellaro, GP. (2009). “Future directions in structural control. ”. *Structural Control and Health Monitoring*, **16**(1), 7–16.

Spencer, BF, Dyke, SJ, Sain, MK, and Carlson, J.D. (1997). “Phenomenological model for magnetorheological dampers. ”. *Journal of engineering mechanics*, **123**(3), 230–238.

Spencer Jr, BF, and Nagarajaiah, S. (2003). “State of the art of structural control. ”. *Journal of Structural Engineering*, **129**, 845–856.

Stark, J., Broomhead, DS, Davies, ME, and Huke, J. (2003). “Delay embeddings for forced systems. II. Stochastic forcing. ”. *Journal of Nonlinear Science*, **13**(6), 519–577.

Suresh, S., Narasimhan, S., and Sundararajan, N. (2008). “Adaptive control of nonlinear smart base-isolated buildings using Gaussian kernel functions. ”. *Structural Control and Health Monitoring*, **15**(4), 585–603.

Terasawa, T., Sakai, C., Ohmori, H., and Sano, A. 2004. “Adaptive identification of MR damper for vibration control. ”. *Pages 2297–2303 of: 43rd IEEE Conference on Decision and Control, 2004. CDC*.

Thai, K., Jabbari, F., and Bobrow, J.E. 1997. “Structural control via semi-active and hybrid control. ”. *In: American Control Conference, 1997. Proceedings of the 1997*, vol. 1.

Wang, S.G., Yeh, HY, and Roschke, P.N. (2001). “Robust control for structural systems with parametric and unstructured uncertainties. ”. *Journal of Vibration and Control*, **7**(5), 753–772.

Wongprasert, N., Symans, MD, *et al.* (2005). “Numerical evaluation of adaptive base-isolated structures subjected to earthquake ground motions. ”. *Journal of engineering mechanics*, **131**, 109–119.

Wu, J.C., Lu, W.C., and Hsu, W.C. (2006). “Implementation of a feasible control design process incorporating robustness criteria for wind-excited high-rise buildings. ”. *Journal of Structural Engineering*, **132**, 89–101.

Xu, B. (2003). “Neural networks for decentralized control of cable-stayed bridge. ”. *Journal of Bridge Engineering*, **8**, 229–236.

Yang, G. 2001. *Large-scale magnetorheological fluid damper for vibration mitigation: modeling, testing and control*. Ph.D. thesis, The University of Notre Dame, Indiana.

Yang, G., Spencer, BF, *et al.* (2002). "Large-scale MR fluid dampers: modeling and dynamic performance considerations. ". *Engineering structures*, **24**(3), 309–323.

Yang, J.N., and Agrawal, A.K. (2002). "Semi-active hybrid control systems for nonlinear buildings against near-field earthquakes. ". *Engineering Structures*, **24**(3), 271–280.

Yang, JN, Wu, JC, and Agrawal, AK. (1995). "Sliding mode control for nonlinear and hysteretic structures. ". *Journal of Engineering Mechanics*, **121**(12), 1330–1339.

Yoshida, O., Dyke, S.J., Giacosa, L.M., and Truman, K.Z. (2003). "Experimental verification of torsional response control of asymmetric buildings using MR dampers. ". *Earthquake Engineering & Structural Dynamics*, **32**(13), 2085–2105.

Zhang, Q., Benveniste, A., and Hogskola, L.T. (1992). "Wavelet networks. ". *IEEE transactions on Neural Networks*, **3**(6), 889–898.

Zhou, L., and Wang, L.X. (2003). "Adaptive fuzzy control for nonlinear building-magnetorheological damper system. ". *Journal of Structural Engineering*, **129**, 905–913.

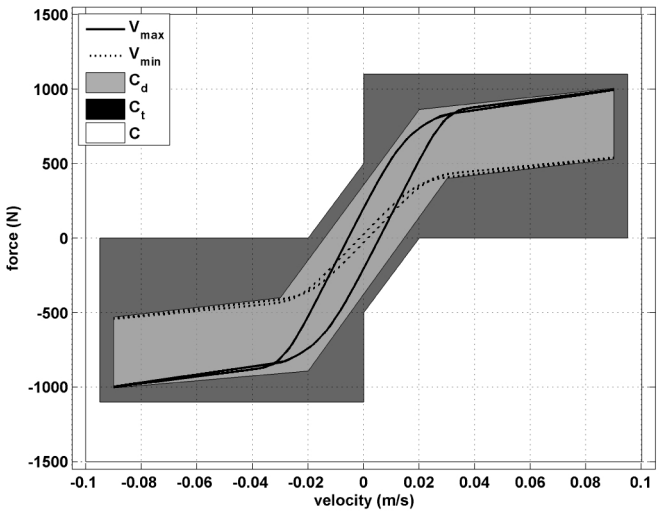

Figure 1: Illustration of controlled regions C, C_t, and C_d for a 1 kN MR damper.

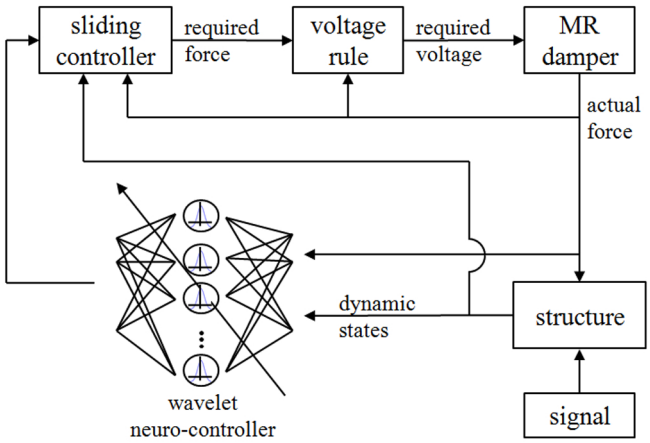

Figure 2: Block diagram of the closed-loop control system.

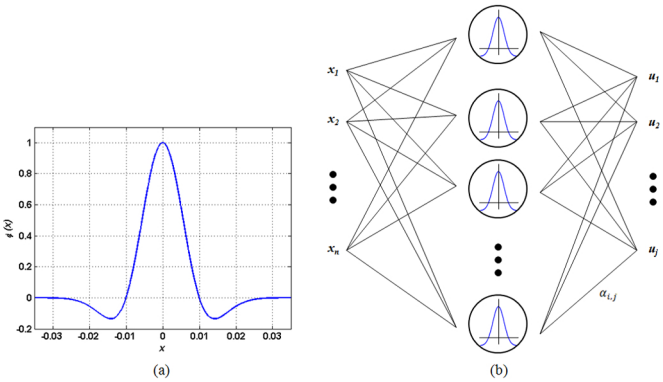

Figure 3: Illustration of: a) a *mexican hat* wavelet with $\mu = 0$ and $\sigma = 0.01$; and b) a wavelet neural network.

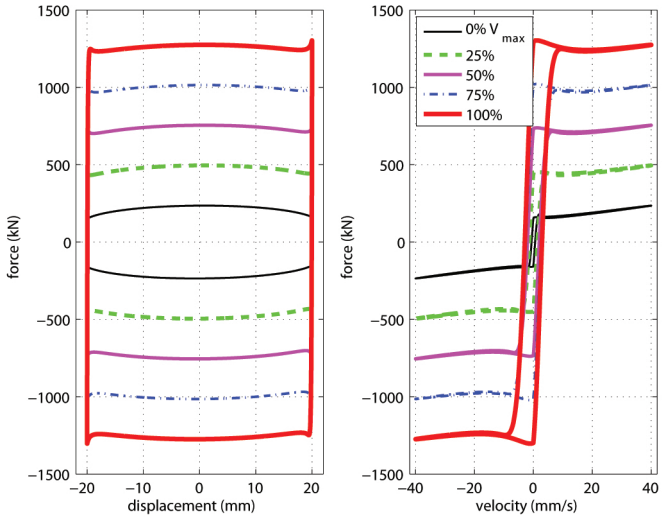

Figure 4: Force-displacement and velocity-displacement plots for a 1350 kN MR damper under a 20 mm harmonic excitation at 0.32 Hz.

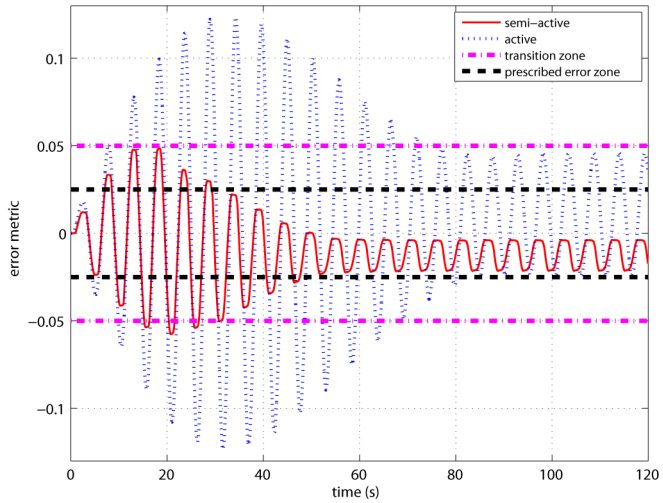

Figure 5: Convergence of the error for the active and semi-active control cases.

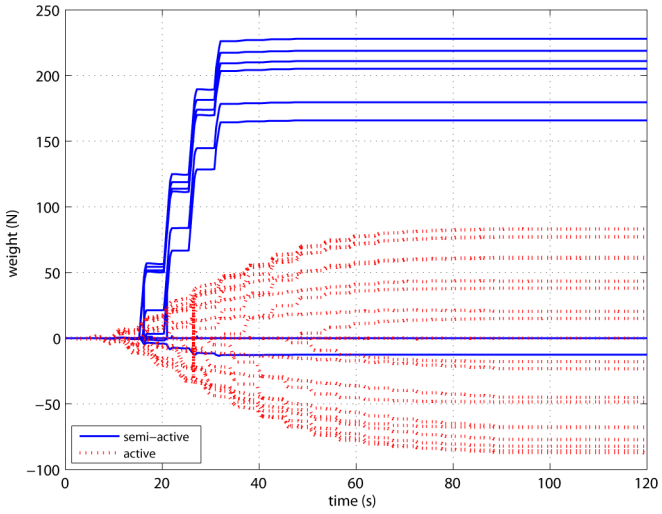

Figure 6: Convergence of the error weights for the active and semi-active control cases.

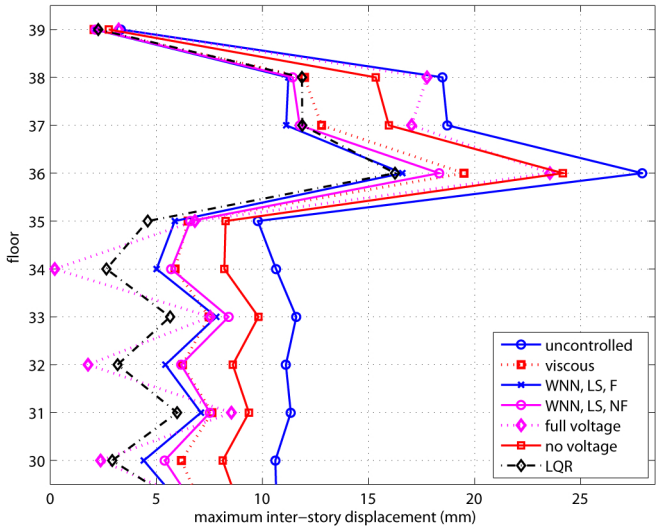

Figure 7: Maximum inter-story displacement profile under various control strategies, earthquake excitation.

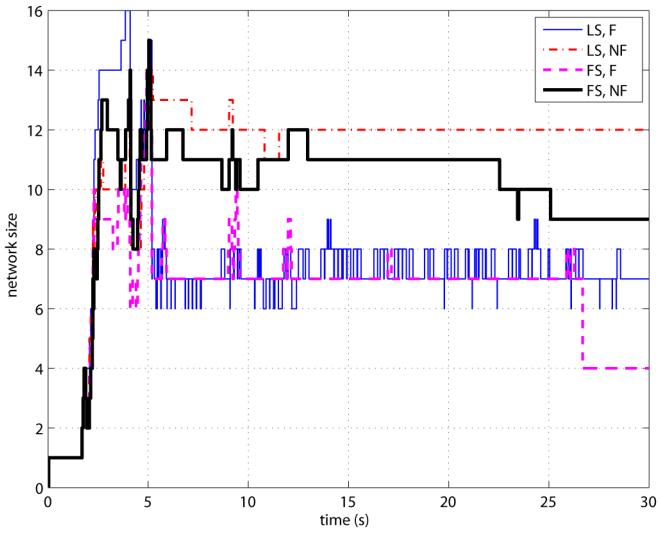

Figure 8: Neural network size under various WNN types for the 15thdamper.

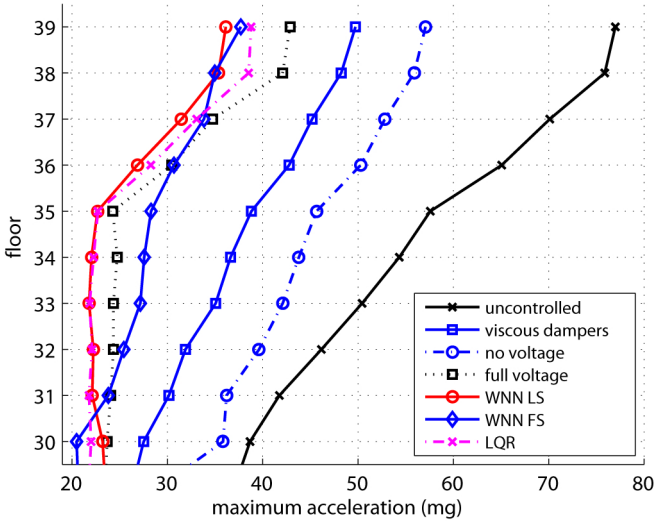

Figure 9: Maximum acceleration profile under various control strategies, wind excitation.

Table 1: Maximum acceleration (mg), active case.

measurement	control delay (ms)						
error (%)	0	40	100	200	400	1000	2000
0	43.1	42.6	41.5	40.2	37.0	49.7	102
5	43.0	42.2	41.2	39.7	36.8	48.7	100
10	41.9	41.5	40.7	39.4	35.8	47.9	106

Table 2: Maximum acceleration (mg), semi-active case.

measurement	control delay (ms)						
error (%)	0	40	100	200	400	1000	2000
0	26.6	27.3	26.5	26.3	26.5	28.6	36.6
5	26.1	26.5	25.8	26.5	27.4	29.2	35.6
10	26.1	26.3	26.3	26.3	27.6	29.9	35.9

Table 3: Maximum inter-story displacement under various control strategies, earthquake excitation.

control strategy	error bound u_b (kN)	maximum inter-story displacement (mm)	reduction (%)
uncontrolled		27.9	
viscous dampers		19.5	30.1
full voltage		23.5	15.8
no voltage		24.2	13.3
WNN, LS, F	225	20.0	28.3
WNN, LS, F	450	17.8	36.2
WNN, LS, F	675	16.6	40.5
WNN, LS, F	900	17.4	37.6
WNN, LS, F	1125	18.4	34.1
WNN, LS, F	1350	18.8	32.6
WNN, LS, NF	675	18.3	34.4
WNN, FS, F	675	17.6	36.9
WNN, FS, NF	675	18.6	33.3
LQR, FS		16.2	41.9

Table 4: Maximum acceleration at the 37thfloor, wind excitation.

control strategy	maximum acceleration $\ddot{x}_{37}$ (mg)	reduction (%)
uncontrolled	70.1	
viscous dampers	45.2	35.5
full voltage	34.8	50.4
no voltage	52.8	24.7
WNN, LS	31.5	55.1
WNN, FS	33.8	51.8
LQR, FS	33.1	52.8